ARTICLES

Journal of Semiconductors
(2020) 41, 082006
doi: 10.1088/1674-4926/41/8/082006

First-principle study of puckered arsenene MOSFET

Hengze Qu, Ziwei Lin, Ruijuan Guo, Xiyu Ming, Wenhan Zhou, Shiying Guo, Xiufeng Song, Shengli Zhang†, and Haibo Zeng†

Key Laboratory of Advanced Display Materials and Devices, Ministry of Industry and Information Technology, College of Material Science and Engineering, Nanjing University of Science and Technology, Nanjing 210094, China

Abstract: Two-dimensional material has been regarded as a competitive silicon-alternative with a gate length approaching sub-10 nm, due to its unique atomic thickness and outstanding electronic properties. Herein, we provide a comprehensively study on the electronic and ballistic transport properties of the puckered arsenene by the density functional theory coupled with nonequilibrium Green's function formalism. The puckered arsenene exhibits an anisotropic characteristic, as effective mass for the electron/hole in the armchair and zigzag directions is 0.35/0.16 m_0 and 1.26/0.32 m_0. And it also holds a high electron mobility, as the highest value can reach 20 045 $cm^2V^{-1}s^{-1}$. Moreover, the puckered arsenene FETs with a 10-nm channel length possess high on/off ratio above 10^5 and a steep subthreshold swing below 75 mV/dec, which have the potential to design high-performance electronic devices. Interestingly, the channel length limit for arsenene FETs can reach 7-nm. Furthermore, the benchmarking of the intrinsic arsenene FETs and the 32-bit arithmetic logic unit circuits also shows that the devices possess high switching speed and low energy dissipation, which can be comparable to the CMOS technologies and other CMOS alternatives. Therefore, the puckered arsenene is an attractive channel material in next-generation electronics.

Key words: first principle; two-dimensional material; electronic properties; arsenene; MOSFET

Citation: H Z Qu, Z W Lin, R J Guo, X Y Ming, W H Zhou, S Y Guo, X F Song, S L Zhang, and H B Zeng, First-principle study of puckered arsenene MOSFET[J]. *J. Semicond.*, 2020, 41(8), 082006. http://doi.org/10.1088/1674-4926/41/8/082006

1. Introduction

As the physical gate length is approaching 10-nm, the silicon-based metal–oxide–semiconductor field-effect-transistors (MOSFETs) are suffering from extremely serious short channel effect, which will greatly degrade the switching performances and cause high static power consumption[1–3]. Two-dimensional (2D) materials with unique atomic thickness showing an outstanding gate-controlling capability have attracted tremendous attention as a promising silicon alternative for next-generation electronics[4–9]. Moreover, the uniform thickness of 2D semiconductors and the surface without dangling bonds can effectively suppress the carrier scattering and contribute to a robust device performance. Besides, the smooth surface and atomic-thickness can also provide a high degree of the vertical integration[10–12].

Nowadays, with the development of the nanotechnology, great progresses have been witnessed in the 2D material-based FET, such as the preparation of graphene, silicene and transition metal dichalcogenides (TMDs) FETs[13–15]. However, it is hard to find a proper candidate to meet the all performance standards of FETs at the same time. For example, even though the graphene FET has a high speed, its metallic characteristic resulted in an unsatisfied switching performance. The sub-10 nm 2D MoS_2 FET with an on/off ratio above 10^7 has been fabricated later, but the on-current is only 250 μA/μm, which is not suitable for high-speed applications[15]. To address these issues, the group-V single element 2D materials composed of phosphorene, arsenene, antimonene and bismuthene with various phase such as puckered (α-phase) and buckled (β-phase) configurations are proposed with an adjustable band gap and high carrier mobility and have been successfully prepared later[16–22]. And their FETs indeed present excellent device performances. The fabricated 2D black phosphorous FETs exhibit ambipolar behavior with the field-effect mobility up to ~10^3 $cm^2V^{-1}s^{-1}$ at room temperature[18], and the first-principle simulation also shows that the α/β-phosphorene, β-arsenene and β-antimonene also possess satisfied performances in both high-performance (HP) and low-power applications at sub-10 nm[23–26]. But there is rare study on the device performance of α-arsenene.

Herein, we systematically evaluate the electronic properties and the ballistic transport performances of the puckered arsenene using the density functional theory (DFT) coupled with nonequilibrium Green's function (NEGF) formalism. The puckered arsenene holds a high electron mobility with the maximum value up to 20 045 $cm^2V^{-1}s^{-1}$. The puckered arsenene FETs with 10-nm channel length (L_{ch}) possess high on/off ratio above 10^5 and steep subthreshold swing (SS) below 75 mV/dec, which have the potential to reach the target of the International Roadmap for Devices and Systems (IRDS) requirements for the HP applications. Furthermore, the benchmarking of the intrinsic devices and the 32-bit arithmetic logic unit (ALU) circuits shows that arsenene FETs have high switching speed and low energy dissipation, which are comparable to the CMOS technologies and other CMOS alternatives.

Correspondence to: S L Zhang, zhangslvip@njust.edu.cn; H B Zeng, zeng.haibo@njust.edu.cn
Received 31 MAY 2020; Revised 7 JUNE 2020.

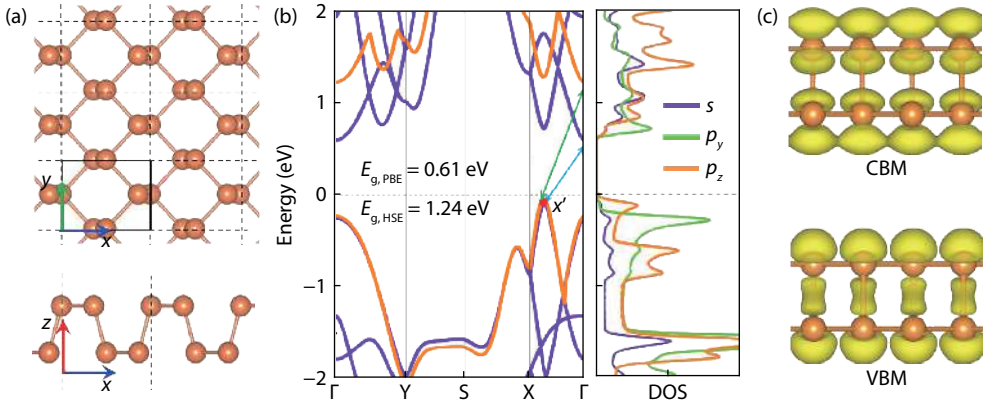

Fig. 1. (Color online) (a) The top and side views of puckered arsenene. (b) The band structure at PBE (purple line) and HSE06 (orange line) level and the orbital-projected density of states of the puckered arsenene. (c) The partial charge density of CBM and VBM.

2. Computational methods

The structure optimization and the electronic properties of puckered arsenene are performed by the Vienna Ab-initio Simulation Package (VASP) code by using the projector augmented wave (PAW) pseudopotential[27]. The Perdew–Burke–Ernzerhof functional of the generalized-gradient approximation (GGA-PBE) considering Grimme's DFT-D2 is adopted[28, 29]. In the self-consistent calculation, the energy cutoff is 500 eV, and the Monkhorst–Pack k-grids of $6 \times 8 \times 1$ is adopted. The energy and force convergence criteria are 10^{-5} eV and 0.005 eV/Å, respectively. A vacuum thickness of 20 Å is used.

The carrier mobility (μ) is calculated using the Takagi formula by the equation[30]:

$$\mu_{2d} = \frac{e\hbar^3 C_{2D}}{k_B T m^* m_d (E_l)^2},$$

in which C_{2D} and E_l represent the elastic moduli and the deformation potential constant, respectively. And they are defined as $C_{2D} = [\partial^2 E/\partial(\Delta l/l_0)^2]/S_0$ and $E_1 = \Delta\varepsilon/(\Delta l/l_0)$, respectively, in which E is the total energy of the unit cell, l_0 is the lattice constant and Δl is the deformation of the l_0 with compression and dilatation, $\Delta\varepsilon$ is the energy change with compression or dilatation strain. m^* is the effective mass in the transport direction and m_d is the average effective mass, which is defined as $m_d = \sqrt{m_x^* m_y^*}$, where m_x^* and m_y^* are the effective mass along the x and y directions, respectively.

The transport properties of puckered arsenene are presented by the Atomistix Toolkit 2019 package[31], as the GGA-PBE functional is adopted to describe the exchange-correlation effect. The drain–source current I_{ds} at a given gate voltage V_g and bias voltage V_{ds} are calculated by the Landauer–Büttiker equation[32]:

$$I_{ds}(V_{ds}, V_g) = \frac{2e}{h}\int_{-\infty}^{+\infty}\{T(E, V_{ds}, V_g) \times [f_s(E-\mu_s) - f_d(E-\mu_d)]\}\,dE,$$

where $T(E, V_{ds}, V_g)$ is the transmission coefficient, $f_{s/d}$ and μ_s/μ_d are the Fermi–Dirac distribution and electrochemical potential of the source/drain. The double-zeta plus polarization basis set is adopted, the density mesh cut-off is 75 Ha and the separation of k-grids is 0.01 Å^{-1}.

3. Results and discussion

The optimized puckered arsenene belongs to orthorhombic system with lattice parameters of x = 4.73 Å, y = 3.68 Å. As shown in Fig. 1(a), arsenene holds a similar configuration to black phosphorene with four atoms in each unit cell, and each As atom is connected to other neighboring three ones exhibiting a puckered honeycomb structure. This honeycomb structure appears as an armchair and a zigzag edge along the x and y directions, respectively.

The simulated band structure of puckered arsenene at PBE level (the purple line) is shown in Fig. 1(b). The conduction band maximum (CBM) is located at Γ point, while the valence band minimum (VBM) occurs at the X′ point (between Γ and X points), leading to an indirect band gap of 0.61 eV. Since the PBE level usually underestimates the band gap, we then use the hybrid functional (HSE06) to provide a more accurate assessment with the value of 1.24 eV. To better understand the properties of the band edge, the orbital-projected density of states (DOS) and the wavefunctions of CBM and VBM (Fig. 1(c)) are also given, which shows that the CBM is comprised by the hybrid states of s-, p_y- and p_z-orbitals, while the VBM is mainly distributed by the p_z-states.

We calculate the effective mass of the band edge, which plays an important role in affecting the carrier mobility and transport performances of the FETs. The band dispersions of the CBM and VBM along armchair and zigzag directions are displayed in Fig. 2. As shown in Figs. 2(a) and 2(b), the band dispersions of electrons along armchair and zigzag directions hold a strong anisotropic characteristic, as the m^* of electron (m_e^*) in the zigzag direction is about four times larger than that in the armchair direction, that is $1.26m_0$ versus $0.35m_0$. The band dispersion of holes in these two directions are shown in Figs. 2(c) and 2(d), which also shows a little anisotropy. The m^* of hole (m_h^*) in the armchair direction is $0.16m_0$, while that in the zigzag direction is $0.32m_0$.

The carrier mobility is one of the most important figures of merits of the material properties toward the realization of an electronic device using puckered arsenene as channel. Here, we provide a qualitative estimation of the carrier mobility by using the deformation potential theory only considering the scatterings of longitudinal acoustic (LA) phonons. Al-

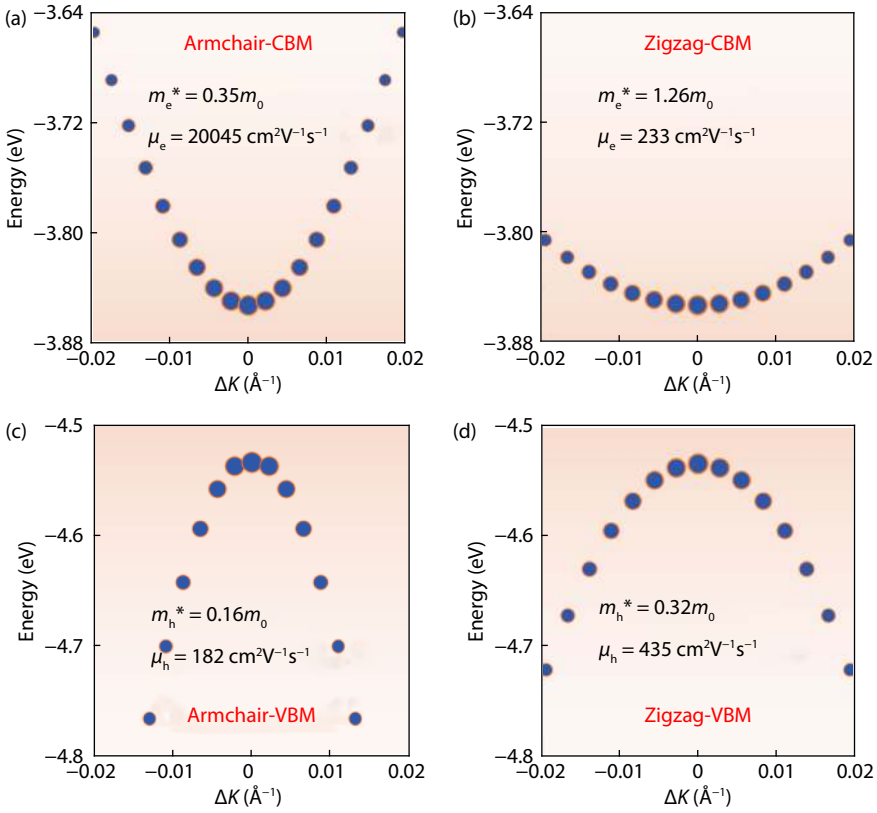

Fig. 2. (Color online) The band dispersions of the CBM along (a) the armchair direction and (b) the zigzag direction, and that of VBM along (c) the armchair direction and (d) the zigzag direction. The corresponding effective mass and carrier mobility are also marked out.

though some other scattering mechanisms such as the acoustic flexural modes (ZA) and optical phonons may also have a strong suppression for the mobility, in MOSFET configurations, the dielectric oxide substrate and gate electrode will suppress the impact of ZA phonons largely and the effect of the optical phonons slightly on the mobility[23, 33]. Therefore, we have not taken them into account here.

On the basis of the Takagi formula, except for the effective mass, another two parameters that play important roles in the mobility are the elastic moduli C_{2D} and the deformation potential constant E_l. The values of C_{2D} in the armchair and zigzag directions are 83.4 and 27.8 N/m, respectively. The values of E_l for electron and hole are anisotropic. Especially for the electrons, the E_l is 0.6 eV in the armchair direction, while it is 3.1 eV in the zigzag direction. For the holes, the values of E_1 along armchair and zigzag directions are 9.3 eV and 2.6 eV, respectively. As a result, due to the ultra-small E_1 and m_e^*, the electron mobility (μ_e^*) in the armchair direction presents an ultra-high value of 20 045 $cm^2V^{-1}s^{-1}$, while that in the zigzag direction is 233 $cm^2V^{-1}s^{-1}$. On the other hand, even though the hole along armchair holds a smaller m^* than that of zigzag, the larger E_1 severely weaken the hole mobility (μ_h^*) and the value of μ_h^* is 182 $cm^2V^{-1}s^{-1}$, while that in the zigzag direction is 435 $cm^2V^{-1}s^{-1}$.

Moreover, it should be noted that except for the coupling with ZA modes and the optical phonons, Takagi formula also neglects the anisotropy of the deformation potential matrix and the inter-valley scatterings. Thereby, the mobility we predicted here should be regarded as the most ideal situation. If a more accurate mobility closer to the experiments is needed, a full *ab initio* approach should be used[33, 34]. We would like to emphasize that our purpose is mainly comparing the mobility to that of other 2D materials using the same method. We note that the mobility of puckered arsenene is very similar to that of black phophornene and much larger than that of MoS_2.

We next present a device simulation based on double-gated MOSFETs. The device models with both armchair and zigzag orientations are selected as the transport directions and are shown in Figs. 3(a) and 3(c), respectively. The intrinsic puckered arsenene as the channel material located between the top and bottom SiO_2 dielectric slabs. The thickness of the SiO_2 is 0.5 nm and the permittivity is 3.9. The source and drain electrodes are highly doped with doping concentration of 3×10^{13} cm^{-2} for both n- and p-type MOSFETs.

To evaluate the potential logic applications of puckered arsenene FETs, we first investigate the transfer characteristics as a function of L_{ch}. The supply voltage V_{dd} is 0.6 V according to the IRDS requirements for 2031 horizons[35]. The *I*–*V* curves of puckered arsenene MOSFET along armchair and zigzag orientations are shown in Figs. 3(b) and 3(d), respectively. Whether the armchair or the zigzag is selected as the transport direction, the p-type MOSFETs always perform a higher drain–source current than the n-type ones. On the other hand, the device performance possesses an obvious anisotropic characteristic. As for both n- and p-type MOSFETs, the armchair-directed devices possess a higher drain-source current than zigzag-directed ones, while the zigzag-directed ones possess a better switching characteristic especially below 10 nm.

The switching characteristic is one of the most important parameters to measure the performance of FETs, which can be clearly described by SS and on/off ratio. SS is defined

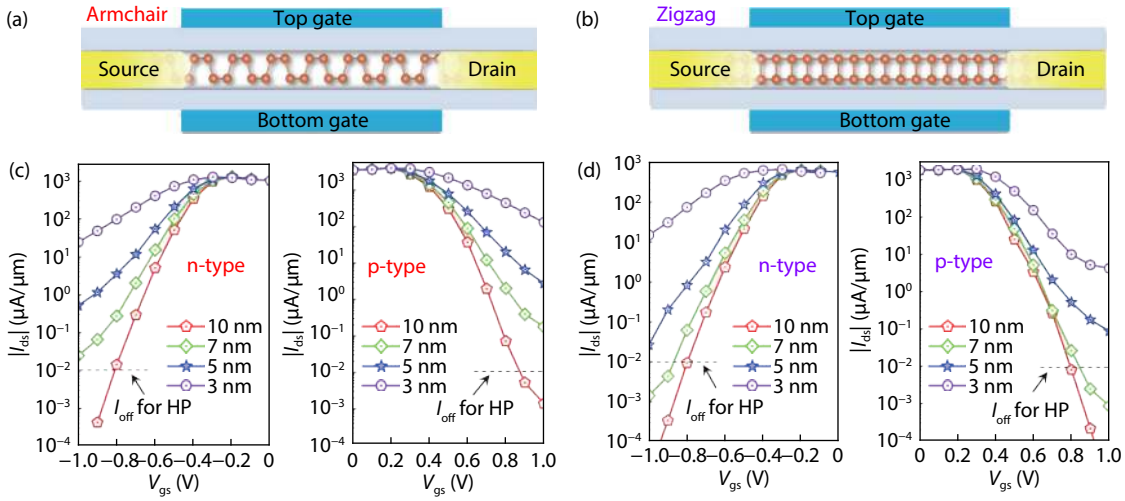

Fig. 3. (Color online) The schematic model of dual-gated puckered arsenene MOSFET along (a) the armchair and (c) zigzag direction. The transfer characteristics for puckered arsenene n- and p-MOSFETs along (b) the armchair and (d) zigzag direction with L_{ch} = 3–10 nm.

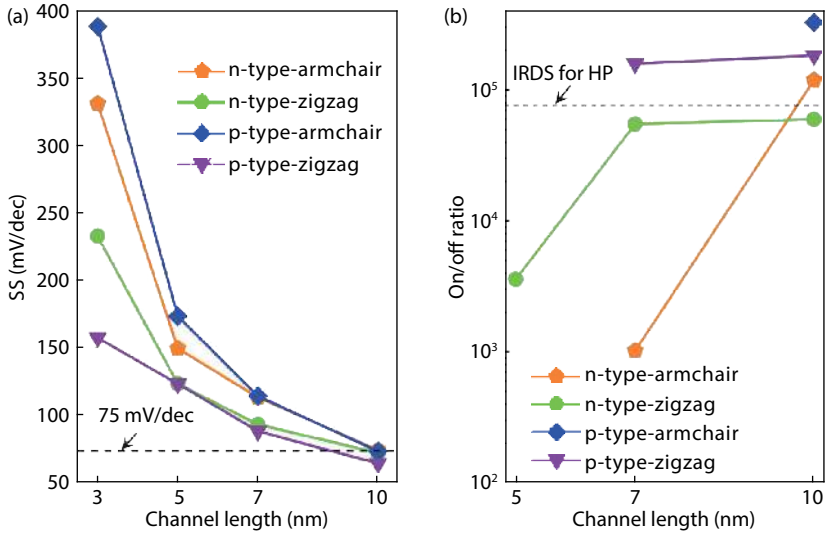

Fig. 4. (Color online) The SS and the on/off ratio as a function of the L_{ch} for the puckered arsenene assessed according to the IRDS requirements for HP applications.

as SS = $(\partial I_g I_{ds}/\partial V_{gs})^{-1}$, which represents the amount of change in the gate voltage as the source-drain current changes by one order of magnitude at the sub-threshold region. A small SS usually means a fast switching speed. The on/off ratio is defined as ratio of on-current (I_{on}) and off-current (I_{off}). The I_{off} is 10 nA/μm according to the IRDS requirements for HP applications, while the I_{on} is ensured by the equation $|V_{gs,\,on} - V_{gs,\,off}| = V_{dd}$, where $V_{gs,\,on}$ and $V_{gs,\,off}$ are the gate–source voltage corresponding to the I_{on} and I_{off}. The SS and the on/off ratio of the puckered arsenene MOSFETs are summarized in Fig. 4. As shown in Fig. 4(a), the SS of all the 10-nm-L_{ch} puckered arsenene MOSFETs is smaller than the IRDS HP requirement of 75 mV/dec, in which the zigzag-directed p-FETs possess the smallest value of 65 mV/dec. As shown in Fig. 4(b), the on/off ratio of other three conditions with 10-nm-L_{ch} except the zigzag-directed n-FET can all fulfill the requirements of the IRDS HP applications in 2031 horizons. This is because the heavier m_e^* in the zigzag direction results in a low drain-source current. Furthermore, as the L_{ch} decreases to 7 nm, although the SS appears a serious degradation, the on/off ratio of the zigzag-directed p-MOSFET can still reach the HP standard.

To reveal the operational principles of the MOSFETs along two different directions, the position resolved local density of states (LDOS) and the spectrum current of 5-nm-L_{ch} n-MOSFETs at V_{gs} = –1 V and 5-nm-L_{ch} p-MOSFETs at V_{gs} = 0.9 V are shown in Fig. 5. As shown in Fig. 5(a), a barrier height Φ_B of 0.18 eV is generated for armchair-directed n-MOSFETs as V_{gs} = –1 V, so that the drain–source current is reduced to 0.8 μA/μm, while the position resolved LDOS of zigzag-directed n-MOSFETs in Fig. 5(b) shows that the V_{gs} of –1 V leads to a higher Φ_B of 0.23 eV, and thereby the drain–source current of the zigzag-directed n-MOSFET decreases to a lower value of 0.02 μA/μm. Except for the difference of the Φ_B, the m^* is the other important parameter that plays an important role in leakage current. The larger the m^*, the smaller the tunneling probability. Therefore, as shown in the spectrum current in Figs. 5(a) and 5(b), the armchair-directed n-MOSFET exhibits a larger specific tunneling current than zigzag-directed n-MOSFET at V_{gs} = –1 V. The anisotropy of the m_h^* is not as signific-

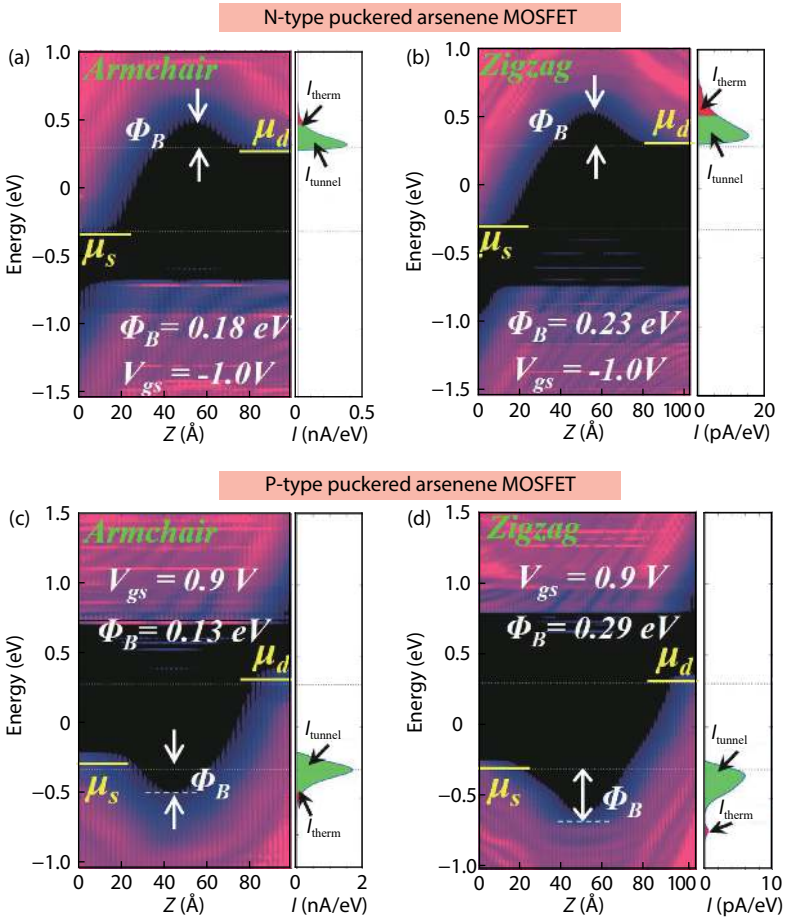

Fig. 5. (Color online) The position resolved LDOS and spectral currents of puckered arsenene n-FETs with 5-nm L_{ch} with the transport direction along (a) armchair and (b) zigzag direction as V_{gs} = −1 V. The position resolved LDOS and spectral current of 5-nm-L_{ch} P-FETs along (c) the armchair and (d) zigzag directions as V_{gs} = 0.9 V.

ant as that of m_e^*, and thereby the proportion of tunneling current in the p-MOSFETs along two different orientations at V_{gs} = 0.9 V has no obvious difference, as shown in spectrum current of Figs. 5(c) and 5(d). For the p-MOSFET, the main reason why the zigzag-directed exhibits a smaller leakage current is the higher Φ_B than the armchair-directed, which is 0.29 versus 0.13 eV.

The intrinsic delay time τ and power dissipation (PDP) are two essential figures of merit ultimately used to evaluate the switching speed and power consumption of FETs. The intrinsic delay time τ and the PDP per width of the puckered arsenene can be calculated by the equation $\tau = \dfrac{Q_{on} - Q_{off}}{I_{on}}$ and PDP $= \dfrac{(Q_{on} - Q_{off})\,V_{dd}}{W}$, respectively, where $Q_{on/off}$ are the total charges of the channel in the on/off-state, and W is the channel width. We calculate the delay time τ and the PDP of the 10-nm-L_{ch} puckered arsenene FETs. The values of delay time τ are 0.054 and 0.091 ps for armchair- and zigzag-directed p-FETs, which are smaller than those of the n-FETs (0.174 ps for armchair-directed n-FET and 0.403 ps for zigzag-directed n-FET). For the PDP, the values are 0.106 and 0.100 fJ/μm for armchair- and zigzag-directed p-FETs, which are also better than those of the n-FETs (0.124 fJ/μm for armchair-directed n-FET and 0.145 fJ/μm for zigzag-directed n-FET). Therefore, for the puckered arsenene, the p-type MOSFETs hold a faster switching speed and a lower power dissipation.

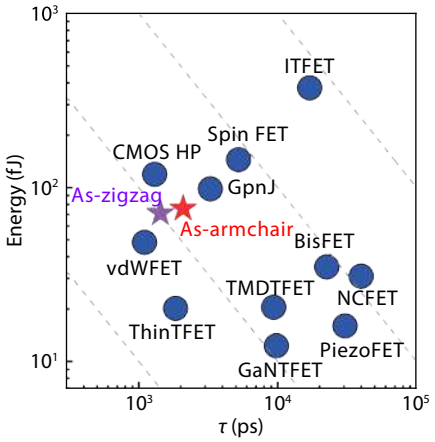

Fig. 6. (Color online) Switching energy versus delay time, τ, for a 32-bit ALU based on puckered arsenene FETs in HP conditions.

Furthermore, we assess the performances of 32-bit ALU circuits based on puckered arsenene FETs considering the interconnects and parasitic capacitances through the software BCB 3.0[36, 37]. The switching energy ($E_{sw} = V_{dd} I_{on} \tau$) versus delay time ($\tau$) for puckered arsenene FET-based 32-bit ALU is shown in Fig. 6. The performance of the zigzag-directed puckered arsenene-based 32-bit ALU (τ/E_{sw} is 1.4 ns/71.4 fJ) is better than the armchair-directed one (τ/E_{sw} is 2.1 ns/75.7 fJ). We further compare them with the other CMOS proposals. The delay time of the puckered arsenene FET-based 32-bit

ALU is comparable with CMOS HP and vdWFET, and their switching energy is much smaller than that of CMOS HP and spin FET. Therefore, puckered arsenene FET is competitive compared with other alternatives at 10-nm node.

4. Conclusion

In summary, we have comprehensively investigated the electronic properties and ballistic quantum transport properties of puckered arsenene using the DFT coupled with NEGF formalism. The puckered arsenene holds an ultra-high carrier mobility with the highest value reaching 20 045 $cm^2V^{-1}s^{-1}$. In the 10-nm node, the puckered arsenene FETs possess a high on/off ratio above 10^5 and a steep SS below 75 mV/dec, which is suitable for HP applications. We also provide a benchmark for the intrinsic puckered arsenene FETs, showing that the zigzag-directed arsenene FETs possess faster switching speeds and low power dissipation. Moreover, the 32-bit ALU circuits simulation results also demonstrate that the arsenene FETs hold promising device performance and are comparable to CMOS technology and some other CMOS alternatives. Therefore, puckered arsenene broadens a promising way in the quest for the novel material that could replace silicon electronics.

Acknowledgements

This work was financially supported by the Training Program of the Major Research Plan of the National Natural Science Foundation of China (91964103), the Natural Science Foundation of Jiangsu Province (BK20180071), the Fundamental Research Funds for the Central Universities (No. 30919011109), and also sponsored by Qing Lan Project of Jiangsu Province, and the Six Talent Peaks Project of Jiangsu Province (Grant No. XCL-035).

References

[1] Chau R, Doyle B, Datta S, et al. Integrated nanoelectronics for the future. Nat Mater, 2007, 6, 810
[2] Franklin A D. Nanomaterials in transistors: From high-performance to thin-film applications. Science, 2015, 349, aab2750
[3] Desai S B, Madhvapathy S R, Sachid A B, et al. MoS_2 transistors with 1-nanometer gate lengths. Science, 2016, 354, 99
[4] Zhang S L, Guo S Y, Chen Z F, et al. Recent progress in 2D group-VA semiconductors: From theory to experiment. Chem Soc Rev, 2018, 47, 982
[5] Guo S Y, Zhang Y P, Ge Y Q, et al. 2D V-V binary materials: Status and challenges. Adv Mater, 2019, 31, 1902352
[6] Zhou W H, Zhang S L, Guo S Y, et al. Designing sub-10-nm metal-oxide-semiconductor field-effect transistors via ballistic transport and disparate effective mass: The case of two-dimensional BiN. Phys Rev Appl, 2020, 13, 044066
[7] Cao W, Kang J H, Sarkar D, et al. 2D semiconductor FETs: Projections and design for sub-10 nm VLSI. IEEE Trans Electron Devices, 2015, 62, 3459
[8] Zhu Z L, Cai X L, Yi S, et al. Multivalency-driven formation of Te-based monolayer materials: A combined first-principles and experimental study. Phys Rev Lett, 2017, 119, 106101
[9] Zhou Z Q, Cui Y, Tan P H, et al. Optical and electrical properties of two-dimensional anisotropic materials. J Semicond, 2019, 40, 061001
[10] Zhou W H, Chen J Y, Bai P X, et al. Two-dimensional pnictogen for field-effect transistors. Res Wash D C, 2019, 2019, 1046329
[11] Novoselov K S, Mishchenko A, Carvalho A, et al. 2D materials and van der Waals heterostructures. Science, 2016, 353, aac9439
[12] Wang S X, Yu Z H, Wang X R. Electrical contacts to two-dimensional transition-metal dichalcogenides. J Semicond, 2018, 39, 124001
[13] Schwierz F. Graphene transistors. Nat Nanotechnol, 2010, 5, 487
[14] Tao L, Cinquanta E, Chiappe D, et al. Silicene field-effect transistors operating at room temperature. Nat Nanotechnol, 2015, 10, 227
[15] Nourbakhsh A, Zubair A, Sajjad R N, et al. MoS_2 field-effect transistor with sub-10 nm channel length. Nano Lett, 2016, 16, 7798
[16] Qiao J S, Kong X H, Hu Z X, et al. High-mobility transport anisotropy and linear dichroism in few-layer black phosphorus. Nat Commun, 2014, 5, 4475
[17] Zhang S L, Yan Z, Li Y F, et al. Atomically thin arsenene and antimonene: Semimetal–semiconductor and indirect-direct band-gap transitions. Angew Chem Int Ed, 2015, 54, 3112
[18] Li L K, Yu Y J, Ye G J, et al. Black phosphorus field-effect transistors. Nat Nanotechnol, 2014, 9, 372
[19] Wang X X, Hu Y, Mo J B, et al. Arsenene: A potential therapeutic agent for acute promyelocytic leukaemia cells by acting on nuclear proteins. Angew Chem Int Ed, 2020, 59, 5151
[20] Zhong M Z, Xia Q L, Pan L F, et al. Thickness-dependent carrier transport characteristics of a new 2D elemental semiconductor: Black arsenic. Adv Funct Mater, 2018, 28, 1802581
[21] Wu X, Shao Y, Liu H, et al. Epitaxial growth and air-stability of monolayer antimonene on $PdTe_2$. Adv Mater, 2017, 29, 1605407
[22] Chen Y B, Chen C Y, Kealhofer R, et al. Black arsenic: A layered semiconductor with extreme in-plane anisotropy. Adv Mater, 2018, 30, 1800754
[23] Pizzi G, Gibertini M, Dib E, et al. Performance of arsenene and antimonene double-gate MOSFETs from first principles. Nat Commun, 2016, 7, 12585
[24] Quhe R G, Li Q H, Zhang Q X, et al. Simulations of quantum transport in sub-5-nm monolayer phosphorene transistors. Phys Rev Appl, 2018, 10, 024022
[25] Wang J, Cai Q, Lei J M, et al. Performance of monolayer blue phosphorene double-gate MOSFETs from the first principles. ACS Appl Mater Interfaces, 2019, 11, 20956
[26] Wang Y Y, Huang P, Ye M, et al. Many-body effect, carrier mobility, and device performance of hexagonal arsenene and antimonene. Chem Mater, 2017, 29, 2191
[27] Kresse G, Furthmüller J. Efficient iterative schemes forab initiototal-energy calculations using a plane-wave basis set. Phys Rev B, 1996, 54, 11169
[28] Perdew J P, Burke K, Ernzerhof M. Generalized gradient approximation made simple. Phys Rev Lett, 1996, 77, 3865
[29] Grimme S, Ehrlich S, Goerigk L. Effect of the damping function in dispersion corrected density functional theory. J Comput Chem, 2011, 32, 1456
[30] Takagi S, Toriumi A, Iwase M, et al. On the universality of inversion layer mobility in Si MOSFET's: Part II-effects of surface orientation. IEEE Trans Electron Devices, 1994, 41, 2363
[31] Atomistix Toolkit vertion 2019.03, Synopsys QuantumWise A/S
[32] Datta S. Quantum transport: atom to transistor. Cambridge: Cambridge University Press, 2005
[33] Gaddemane G, Vandenberghe W G, van de Put M L, et al. Theoretical studies of electronic transport in monolayer and bilayer phosphorene: A critical overview. Phys Rev B, 2018, 98, 115416
[34] Poncé S, Margine E R, Giustino F. Towards predictive many-body calculations of phonon-limited carrier mobilities in semiconductors. Phys Rev B, 2018, 97, 121201
[35] International Roadmap for Devices and Systems, 2018 edition. https://irds.ieee.org/editions/2018 (accessed May 20, 2019)
[36] Nikonov D E, Young I A. Overview of beyond-CMOS devices and a uniform methodology for their benchmarking. Proc IEEE, 2013, 101, 2498
[37] Nikonov D E, Young I A. Benchmarking of beyond-CMOS exploratory devices for logic integrated circuits. IEEE J Explor Solid-State Comput Devices Circuits, 2015, 1, 3